



# The evolution of rock friction is more sensitive to slip than elapsed time, even at near-zero slip rates

Pathikrit Bhattacharya<sup>a,1</sup>, Allan M. Rubin<sup>b</sup>, Terry E. Tullis<sup>c</sup>, Nicholas M. Beeler<sup>d</sup>, and Keishi Okazaki<sup>e,f</sup>

Edited by James Rice, Harvard University, Cambridge, MA; received November 3, 2021; accepted May 17, 2022

Nearly all frictional interfaces strengthen as the logarithm of time when sliding at ultra-low speeds. Observations of also logarithmic-in-time growth of interfacial contact area under such conditions have led to constitutive models that assume that this frictional strengthening results from purely time-dependent, and slip-insensitive, contact-area growth. The main laboratory support for such strengthening has traditionally been derived from increases in friction during “load-point hold” experiments, wherein a sliding interface is allowed to gradually self-relax down to subnanometric slip rates. In contrast, following step decreases in the shear loading rate, friction is widely reported to increase over a characteristic slip scale, independent of the magnitude of the slip-rate decrease—a signature of slip-dependent strengthening. To investigate this apparent contradiction, we subjected granite samples to a series of step decreases in shear rate of up to 3.5 orders of magnitude and load-point holds of up to 10,000 s, such that both protocols accessed the phenomenological regime traditionally inferred to demonstrate time-dependent frictional strengthening. When modeling the resultant data, which probe interfacial slip rates ranging from  $3 \mu\text{m} \cdot \text{s}^{-1}$  to less than  $10^{-5} \mu\text{m} \cdot \text{s}^{-1}$ , we found that constitutive models where low slip-rate friction evolution mimics log-time contact-area growth require parameters that differ by orders of magnitude across the different experiments. In contrast, an alternative constitutive model, in which friction evolves only with interfacial slip, fits most of the data well with nearly identical parameters. This leads to the surprising conclusion that frictional strengthening is dominantly slip-dependent, even at subnanometric slip rates.

physics of friction | earthquake physics | experimental rock mechanics

Frictional surfaces across a wide range of materials are known to strengthen at low sliding rates. In the laboratory, this strengthening is often explored through slide–hold–reslide experiments, where a sample previously driven at a constant sliding speed is perturbed by abruptly holding the external load at fixed displacement or a fixed, low stress level (1–8). In the former protocol, which we call a load-point hold, slip along the frictional interface continues at an ever-decreasing rate as the mechanical system (testing machine plus sample) elastically unloads and the shear stress on the frictional interface decreases. For hold durations longer than a few seconds, the static friction peak observed upon resliding at the prehold rate has been shown to increase as the logarithm of the hold duration, across a wide range of materials, including rocks (1, 4, 5, 8, 9) (*SI Appendix*, Fig. S1).

In providing a physical explanation for these observations of frictional strengthening, reference has often been made to the similarly logarithmic-in-time growth of interfacial contact area (in transparent polymer glasses and plastics) during periods of little to no slip (10, 11). The connection of frictional strength to contact area dates back to Bowden and Tabor (12), who imagined frictional strength of an interface ( $\tau_f$ ) as the product of an average velocity-dependent contact strength ( $\tau_c$ ) (6) and the ratio of the real contact area to the total contact area ( $\Sigma_r$ ):  $\tau_f = \tau_c \Sigma_r$ . Logarithmic growth of contact area is expected if contacts deform via thermally activated creep at normal stresses close to the indentation hardness of the sample (6, 8, 13). In the Bowden and Tabor view, this contact-area growth then leads to a logarithmic-in-time increase in friction measured relative to the steady-state prehold and posthold sliding rate. One consequence of this view is that the strength increase during the hold portion of slide–hold–reslides should be predictable from the hold duration alone and be insensitive to the small amount of interfacial slip that accumulates during the hold (4).

The largely empirical rate–state friction (RSF) equations are widely used to model such time-varying friction phenomenology in rock (4, 5, 14) and a diverse set of industrial materials (6, 15–19). However, the two most widely used versions offer opposing views of the importance of slip for friction evolution. The more commonly used Aging formulation (1, 14) predicts that frictional strengthening loses all sensitivity to slip whenever the interface is subjected to a sufficiently large and rapid decrease in slip rate. In the limit

## Significance

For many decades, frictional strength increase at low slip rates has been ascribed to time-dependent contact-area growth across the sliding interface. As a result, phenomenological models that correctly predict contact-area growth, as observed in laboratory experiments, have also been widely assumed to be appropriate descriptors of frictional strength evolution. We present experiments that impose more than 5-orders-of-magnitude slip-rate reductions on granite to show that frictional strength evolution in these rocks unequivocally refutes such models. Instead, the data suggest that, even at subnanometric slip rates, frictional strength dominantly evolves with accrued slip. This remarkable slip-sensitivity of friction requires changes of intrinsic strength of the interface with slip that are absent from popular conceptual models of friction at the microscopic contact scale.

Author contributions: P.B., A.M.R., and N.M.B. designed research; P.B., A.M.R., T.E.T., and K.O. performed research; P.B. analyzed data; and P.B., A.M.R., T.E.T., N.M.B., and K.O. wrote the paper.

The authors declare no competing interest.

This article is a PNAS Direct Submission.

Copyright © 2022 the Author(s). Published by PNAS. This article is distributed under [Creative Commons Attribution-NonCommercial-NoDerivatives License 4.0 \(CC BY-NC-ND\)](https://creativecommons.org/licenses/by-nc-nd/4.0/).

<sup>1</sup>To whom correspondence may be addressed. Email: pathikritb@niser.ac.in.

This article contains supporting information online at <https://www.pnas.org/lookup/suppl/doi:10.1073/pnas.2119462119/-DCSupplemental>.

Published July 20, 2022.

of a truly stationary interface, it implies strengthening as the logarithm of time, even in the absence of slip. When viewed in conjunction with the evidence for log-time growth of contact area across stationary interfaces, this is consistent with the Bowden and Tabor view of contact area being the primary determinant of macroscopic strength. Its more empirical alternative—the Slip formulation—instead predicts no strengthening in the absence of sliding and retains slip-sensitivity at all slip rates (20).

Over the last three decades, phenomenological details of frictional strengthening derived from laboratory slide-hold-reslide experiments have been widely interpreted as supporting the Aging-formulation view—that frictional strengthening loses sensitivity to slip under the extreme slip-rate reductions imposed during load-point holds (3–7, 21). In contrast, friction evolution in response to less extreme, but still 1- to 2-orders-of-magnitude, velocity-step decreases in the laboratory demonstrates strengthening over a characteristic slip distance independent of the final slip rate, a feature consistent with the slip dependence of friction predicted by the Slip formulation (22, 23). Therefore, somewhat paradoxically, while load-point holds and large velocity-step decreases both probe the evolution of friction following large reductions in slip rate, the traditional interpretations of these two protocols seem to provide entirely contradicting versions of the processes underlying frictional strengthening.

One resolution to this paradox is to hypothesize a rate-sensitive transition from slip- to time-dependent strengthening that is hidden within the orders-of-magnitude gap in the slip rates typically probed by these two sliding protocols (24). To test this hypothesis, and to eliminate any effects of differences in samples or experimental conditions, we ran a suite of extremely large velocity-step decreases (0.5 to 3.5 orders of magnitude between  $3 \mu\text{m} \cdot \text{s}^{-1}$  and  $0.001 \mu\text{m} \cdot \text{s}^{-1}$ ) and load-point holds (of durations 10 to  $10^4$  s) on an initially bare granite sample, all during the same experimental run. For our experimental conditions, these extreme velocity-step decreases reach slip rates as low as those accessed during hold durations of a few 100 s—durations comfortably larger than those above which time-dependent strengthening has been widely inferred (4, 5, 11). Crucially, this means that the data from either the velocity-step or slide-hold protocols are independently sufficient to test for a rate-sensitive transition from slip- to time-dependent strengthening with decreasing slip speed.

Contrary to conventional wisdom, we find that the data derived from both sliding protocols support dominantly slip-dependent strength evolution, even for nearly stationary surfaces (minimum estimated slip speeds  $< 10^{-5} \mu\text{m/s}$ ). In particular, we find that the Slip equation describes most of the data quite well using nearly identical parameters, even across these many-orders-of-magnitude variations in slip rate. In contrast, the Aging equation produces worse fits to the data, while also requiring orders-of-magnitude variations in the inferred RSF parameters across the diverse sliding conditions. We trace these failures of the Aging equation back to one central flaw—its prediction that strength increases primarily with time, and not slip, following large, rapid decreases in slip rate.

## RSF and Probing Strengthening with Velocity Steps and Holds

Within the RSF framework (1, 5, 9, 20, 25), the friction coefficient is expressed as a function of the sliding rate ( $V$ ) and the “state variable” ( $\theta$ ) describing the state of the sliding surface. In its simplest form, the friction equation is:

$$\mu = \frac{\tau_f}{\sigma} = \mu_* + a \ln\left(\frac{V}{V_*}\right) + b \ln\left(\frac{V_* \theta}{D_c}\right), \quad [1]$$

where  $\mu$  is the friction coefficient,  $\tau_f$  is the shear stress during sliding,  $\sigma$  is the normal stress, and the parameters  $a$  and  $b$  determine the amplitude of the log velocity and log-state dependence of friction.  $\mu_*$  is the steady-state friction value at an arbitrary reference sliding speed  $V_*$ . At moderate temperatures,  $a$  and  $b$  are of order 0.01 (26), much smaller than the nominal friction value  $\mu_*$  of  $\sim 0.6$  to 0.8. Despite being small, the rate- and state-dependence of friction is important; it determines, for example, whether surfaces slide stably at the applied loading rate ( $a > b$ ; referred to as “velocity-strengthening”), or potentially undergo stick-slip motion ( $a < b$ ; “velocity-weakening”). The velocity dependence is universally positive ( $a > 0$ ) and is generally interpreted to result from a thermally activated Arrhenius process associated with breaking chemical bonds between asperities that bridge the sliding surface (27, 28). The source of the state-dependence is poorly understood. Despite apparent similarities in the phenomenology of state evolution among many classes of solids, including rock, glass, metal, paperboard, wood, plastics, and rubber (6, 8, 10, 16, 18), it is not at all obvious that the physical and chemical processes underlying this evolution are shared.

It is commonly assumed that the time derivative of the state variable,  $\dot{\theta}$ , can be written as functions of the current values of  $V$  and  $\theta$  only, although this assumption might be somewhat restrictive (20). For decades, the most widely used forms of the state-evolution equations have been:

$$\text{Aging (Dieterich) Equation: } \dot{\theta} = 1 - \frac{V\theta}{D_c}, \quad [2a]$$

$$\text{Slip (Ruina) Equation: } \dot{\theta} = -\frac{V\theta}{D_c} \ln\left(\frac{V\theta}{D_c}\right), \quad [2b]$$

where  $D_c$  is a characteristic slip scale, often associated with the size of contacting asperities on the interface (2, 20). State here has units of time.

At steady-state sliding ( $\dot{\theta} = 0$ ), both equations yield  $V\theta/D_c = 1$ , or  $\theta = D_c/V$ , consistent with the interpretation that at steady-state  $\theta$  reflects “contact age.” For both equations,  $V\theta/D_c < 1$  leads to  $\dot{\theta} > 0$ . We refer to this as being “below steady state.” The increase in friction resulting from the below-steady-state increase in  $\theta$  is what we mean by frictional strengthening.

The Aging and Slip formulations differ in their predictions for strengthening when  $V\theta/D_c$  drops to values much smaller than one. Given that neither equation allows for instantaneous changes in state, such “far below steady-state” regimes can be attained via sufficiently large and rapid reductions in slip rate from steady-state sliding. In response, state evolution under the Aging formulation loses all sensitivity to slip rate, as Eq. 2a reduces to  $\dot{\theta} \sim 1$ . State then evolves purely as a function of time and, again, invites the interpretation that state is contact age. Note that cessation of slip is not required to satisfy  $\dot{\theta} \sim 1$ ; it is sufficient that  $\theta \ll D_c/V$ . In contrast, under the Slip formulation, the rate of state evolution decreases to progressively smaller values as the size of the velocity reduction increases, with no strengthening in the limit  $V \rightarrow 0$ . Nevertheless, in practice, due to the finite compliance of testing machines, slip speed never decays to zero. Under these circumstances, both formulations predict an approximately logarithmic-in-time increase in frictional strength during long-duration load-point holds (strictly so under the Aging formulation, as  $\dot{\theta} \sim 1$ ) (20, 23). Therefore, that frictional strength increases nearly logarithmically with hold duration in slide-hold-slide experiments does not by itself distinguish between evolution of friction with slip or with elapsed time.

The slip-sensitivity of strengthening was explored by Beeler et al. (4) in an experiment consisting of the same sequence of holds at two very different machine stiffnesses. They showed that the rate of increase in peak friction with log-hold duration was independent of the adopted stiffness and, hence, independent of the very different amounts of slip that accrued during the holds. Beeler et al. interpreted these data as supporting time-dependent strengthening during holds. Together with the discovery of logarithmic-in-time contact-area growth (10, 11) and the correspondence between Aging-law-style time-dependent strengthening and contact-area growth when viewed within the Bowden–Tabor picture (8, 13), the experiments of Beeler et al. (4) have been cited as evidence in support of time-dependent contact-area growth, leading to frictional strengthening during holds.

The strongest evidence against this viewpoint, and for the importance of slip in determining friction evolution far below steady state, comes from velocity-step experiments, as mentioned before. The Slip formulation, in fact, was introduced because it matches so well the results of laboratory velocity-step experiments, where friction is observed to approach its future steady-state value as roughly a decaying exponential over a characteristic slip distance ( $D_c$ ), independent of the final slip speed, as well as the magnitude and sign of the velocity step (20). For velocity-step decreases, this clearly calls into question the universality of the hypothesis that frictional strengthening far below steady state depends upon time rather than slip.

Recently, Bhattacharya et al. (23) resolved some of this conundrum by reinterpreting the slide–hold–reslide experiments of Beeler et al. Bhattacharya et al. showed that the Slip formulation can model the stiffness-independence of the healing rate inferred from the peak friction data as well as the Aging formulation, albeit over a narrower range of parameter values. Moreover, the holds preceding these peak friction values exhibit strongly stiffness-dependent stress-relaxation rates, which, with constant RSF parameters, cannot be captured by the Aging formulation, but are well modeled by the Slip formulation. However, this does not rule out the possibility that this apparent failure of the Aging formulation has nothing to do with the prescription of state evolution and is, instead, just an artifact of the assumption of velocity-independent, constant RSF parameters. To explore the latter possibility, it is necessary to increase the size of the velocity-step decreases and drop the target velocity into the range accessed by moderately long holds. This will effectively allow any rate-dependence of the RSF parameters to be detected by the rate steps alone.

The Tullis rotary shear apparatus at Brown University (25, 29, 30) is uniquely suited to our purpose, given that it can be servo-controlled by using a resolver near the sliding interface to artificially stiffen the machine to around 30 to 40 times its natural stiffness (4, 23). All the experiments reported in this paper make use of this stiffened setting. Increasing the apparatus stiffness ensures that a large velocity step imposed at the load point is translated to the sample with greater fidelity. This maximizes the departure from steady state for a given velocity-step decrease at the load point (31), which facilitates distinguishing slip- from time-dependence when inverting the resulting friction data.

As we will show, the dataset generated from the experiments described herein provides sufficient diagnostic power to join a growing body of work, referenced later, suggesting that 1) frictional “state” is not synonymous with contact area, and 2) slip is essential to frictional strengthening, as observed in laboratory experiments on rocks.

**Large Velocity-Step Decreases on a Stiff Apparatus.** The velocity steps were carried out at 25-MPa normal stress on a hollow,

cylindrical sample of Westerly granite with outer and inner diameters of 54 and 44 mm (for details of the apparatus and sample, see *SI Appendix*, Figs. S2 and S3). The sample was initially ground flat and then roughened at a fine scale by using 60-grit grinding compound. We report experimental results only after about 120 mm of slip. At these large amounts of slip, the sample reached a stable, quasi-constant, steady-state velocity-weakening value of  $a - b \approx -0.003$  (*SI Appendix*, Fig. S6). Previous studies on the same apparatus under similar conditions have shown that, during the accumulation of  $\sim 40$  to 100 mm of slip, a 70- to 100- $\mu\text{m}$ -thick layer of gouge develops on Westerly granite samples, with the total shear being accommodated in a narrow (20 to 30  $\mu\text{m}$  wide), quasi-planar, shear zone within this gouge (29).

To estimate the slip velocity from the displacement measured by the resolver (what we term the “load point”), we must correct for elastic deformation of the intervening material (about 5 mm of rock plus a thin layer of glue). The elastic stiffness  $k$  (expressed as friction change per differential slip distance between the surface and the load point) was determined to be  $0.065 \mu\text{m}^{-1}$  (*Materials and Methods* and *SI Appendix*, Fig. S4). Assuming homogeneous shear stress and slip distribution on the sliding interface, the elastic relation between the measured shear traction on the sample ( $\tau$ ), the load-point displacement ( $\delta_{\text{lp}}$ ), and the surface slip ( $\delta$ ), is

$$\tau = k\sigma(\delta_{\text{lp}} - \delta). \quad [3]$$

Taking the time derivative enables us to estimate the slip speed  $V$  in terms of the servo-controlled load-point velocity  $V_{\text{lp}}$  and the time-derivative of the shear load:

$$V = V_{\text{lp}} - \frac{\dot{\tau}}{k\sigma}. \quad [4]$$

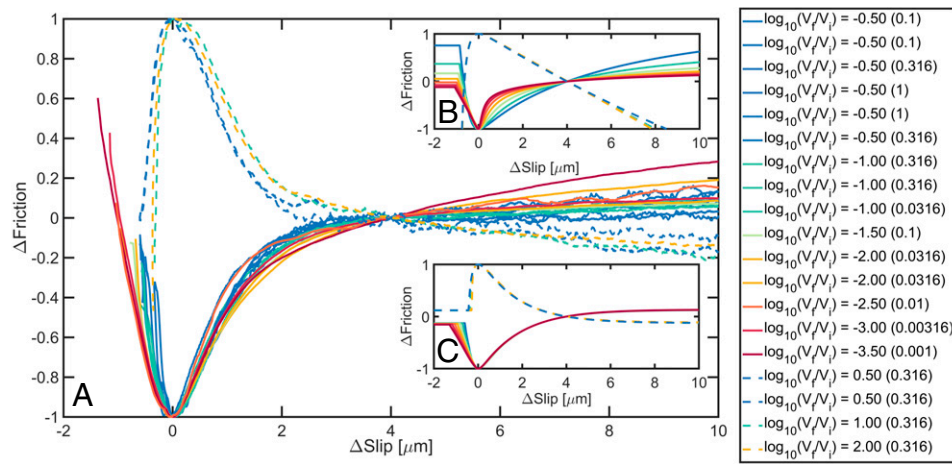
Because the surface is always sliding, even at the end of the longest load-point holds ( $V = 0.02 \pm 5\% \text{ nm} \cdot \text{s}^{-1}$  at the end of our 10,000-s holds; *SI Appendix*, Fig. S5), and because slip speeds and accelerations are small enough that inertia is negligible, we can relate changes in friction to changes in shear load throughout these experiments via  $\Delta\mu = \Delta\tau/\sigma$ .

Fig. 1*A* shows friction data from a large number of velocity-step decreases and increases. In these tests, the sample is initially run to steady state at a velocity  $V_{\text{lp}} = V_i$ , and then  $V_{\text{lp}}$  is changed to  $V_f$  over  $\sim 0.02$  s. When servo-controlling off the near-fault resolver, we were able to impose sliding rates of 3 to  $0.001 \mu\text{m} \cdot \text{s}^{-1}$ , allowing velocity jumps of up to 3.5 orders of magnitude. Previously published jumps have been limited to 2 orders of magnitude.

Each friction curve in Fig. 1*A* has been normalized by the amplitude of its total change from its extremum to its value measured at  $4 \mu\text{m}$  of slip, with slip defined as zero at the extremum. Over this initial  $4 \mu\text{m}$  of postminimum slip, the plot clearly shows that frictional strength evolves over a length scale that is independent of both the step size and final slip speed  $V_f$ .

For comparison, we have plotted numerical simulations of velocity-step decreases using both the Aging formulation (Fig. 1*B*) and the Slip formulation (Fig. 1*C*). These simulations were run with the appropriate stiffness and  $a$ ,  $b$ , and  $D_c$  values derived by fitting the first  $3 \mu\text{m}$  of the poststep friction evolution from a subset of the velocity steps shown in Fig. 1*A* (*Materials and Methods*; *SI Appendix*, Figs. S6, S7, and S8; and Table 1).

Note that in both the observations and the simulations, after a step decrease in  $V_{\text{lp}}$ , the stress first decreases to a minimum before increasing to its future steady-state value at  $V = V_f$ . In the simulations, the steep stress decay prior to the minimum is dominated by changes in the  $a \ln(V/V_*)$  term in [1]



**Fig. 1.** (A) Large velocity-step decreases and increases on initially bare granite. Beyond 120 mm of total slip, 16 velocity-step decreases and 13 increases were carried out spanning 0.5 to 3.5 orders of magnitude. This plot shows 15 of these step decreases and 4 of the increases; the remainder are shown in *SI Appendix*, Fig. S20. The legend shows  $\log_{10}(V_f/V_i)$  values coded by color; in parentheses are the final slip speeds  $V_f$  in  $\mu\text{m/s}$ . The slip is set to zero at the stress minimum (or maximum for the step increases). The data are smoothed over 0.2  $\mu\text{m}$  for the step-downs and over 0.4  $\mu\text{m}$  for the step-ups. The main panel shows the friction normalized by its change between 0 and 4  $\mu\text{m}$  of slip. *B* and *C* show the evolution of friction for the range of step increases and decreases shown in *A* (colors denote step-sizes as in *A*) for the Aging and Slip formulations, respectively. The modeled friction variations are normalized identically to the data in *A*. The parameters used for the Aging and Slip simulations are derived from fitting the velocity-step decreases (*SI Appendix*, Figs. S7 and S8). The modeled time series is smoothed identically to the data. In *A*, the friction values for the two largest step decreases begin well above zero because of the normalization scheme (the friction by 4  $\mu\text{m}$  of slip remains well below its future steady-state value; Fig. 2*A*).

(a rapid velocity drop at relatively constant state), whereas the subsequent steep stress increase is dominated by changes in the  $b \ln(V_*\theta/D_c)$  term (state increases at nearly constant  $V = V_f$ ; *SI Appendix*, Figs. S7 and S8). Therefore, across the many orders-of-magnitude poststep slip rate ( $V_f$ ) variations in Fig. 1*A*, friction evolution for the first 4  $\mu\text{m}$  of slip following the stress minimum represents frictional strengthening over elapsed times that vary by more than 3 orders of magnitude. This suggests that the collapse (for these short slip distances) of the whole suite of postminimum velocity-step data onto nearly the same curve implies the primacy of interfacial slip accumulation over time elapsed in determining this strengthening. The Slip formulation inherently captures this phenomenology, given its prediction that friction evolves to steady state over a characteristic slip scale, independent of the step size and  $V_f$  (20) (Fig. 1*C*).

On the other hand, following a large velocity-step decrease, the Aging formulation predicts strengthening over length scales that decrease dramatically as the size of the velocity step increases (note this feature in the progression of colors subsequent to the stress minimum in Fig. 1*B*). For velocity decreases that push

the interface far below steady state ( $V\theta/D_c \ll 1$ ), the rate of friction change with slip  $d\mu/d\delta$  increases almost as rapidly, with increasing velocity reduction as the velocity ratio  $V_i/V_f$  (*SI Appendix*, section 4). This is in clear contradiction with the data.

The velocity-step data from Fig. 1 are shown again as nonnormalized friction versus slip in Fig. 2*A*, with the changes in friction referenced to the prestep steady-state level. The corresponding simulation results using the Aging and Slip formulations are shown in Fig. 2 *D* and *E*. Notably, for the experimental data, the amplitude of the stress minimum  $\Delta\mu_{\min}$  increases linearly with the logarithm of the size of the velocity step (Fig. 2 *A*, *Inset*), with a slope of around  $-0.01$ . Using parameters derived from fits to the velocity-step decreases (Table 1), Slip-formulation simulations also show a linear growth in  $\Delta\mu_{\min}$  with log step size with a slope  $\sim -0.009$  (Fig. 2*C*). The data also show (Fig. 2*A* and *SI Appendix*, Fig. S13) that the slip accumulated between the start of the velocity step and the friction minimum increases quasi-linearly with the log of the step size, again consistent with the Slip-formulation simulations (Fig. 2*E*).

The Aging formulation, on the other hand, predicts a non-linear relationship between  $\Delta\mu_{\min}$  and log step size with the rate of increase in  $\Delta\mu_{\min}$  decreasing systematically with larger steps (Fig. 2*B*). In general, any increase in state (strengthening) between the onset of the velocity step and the friction minimum reduces the eventual amplitude of  $\Delta\mu_{\min}$ . For large velocity-step decreases ( $V_f/V_i \ll 1$ ),  $V\theta/D_c \ll 1$  prior to the friction minimum. Under an Aging-style formulation, this leads to  $\dot{\theta} \sim 1$  and a much larger increase in  $\theta$  prior to the friction minimum than for the Slip formulation. This leads to considerable shallowing of the curve of  $\Delta\mu_{\min}$  with decreasing  $V_f/V_i$ .

Fig. 2 *F–L* show Slip-formulation fits to the first 3  $\mu\text{m}$  of poststep friction evolution of one each of the different step sizes in our experimental suite (all steps are fit in *SI Appendix*, Fig. S9). Unlike the fits used to infer the RSF parameters for the simulations in Figs. 1*C* and 2 *C* and *E*, the fits in Fig. 2 *F–L* allow different values of  $a$  and  $D_c$  (while fixing  $a - b = -0.003$ ) for every velocity step shown in Fig. 1*A*. These fits reveal that the Slip formulation requires almost no variation in  $a$ , and  $D_c$  variations

**Table 1. Rate-state parameters from fitting the friction data**

Type	$V_i$	EE	TH, s	$a$	$b$	$D_c$	Fig. no.
Steps*	—	A	—	0.014	—	10.05	<a href="#">S8</a>
Steps	—	A	—	0.022	0.018	0.99	<a href="#">S8</a>
Holds*	0.032	A	10,000	0.012	—	84.85	<a href="#">4B</a>
Holds*	0.32	A	1,000	0.013	—	103.40	<a href="#">4A</a>
Holds*	0.32	A	3,163	0.012	—	3055.33	<a href="#">S16</a>
Holds*	1.0	A	1,000	0.013	—	663.66	<a href="#">4C</a>
Steps	—	S	—	0.013	0.016	2.07	<a href="#">S7</a>
Holds*	0.032	S	10,000	0.014	—	1.99	<a href="#">4E</a>
Holds*	0.32	S	1,000	0.015	—	2.10	<a href="#">4D</a>
Holds*	0.32	S	3,163	0.014	—	4.63	<a href="#">S16</a>
Holds*	1.0	S	1,000	0.015	—	3.43	<a href="#">4F</a>

EE denotes choice of evolution equation: A for Aging, S for Slip. TH denotes the longest hold duration fit as part of this series. Fig no. denotes the figure number for the listed fits.  $V_i$  values are in  $\mu\text{m} \cdot \text{s}^{-1}$ , and  $D_c$  are in  $\mu\text{m}$ .

\* denotes  $a - b = -0.003$  constraint imposed on these fits.

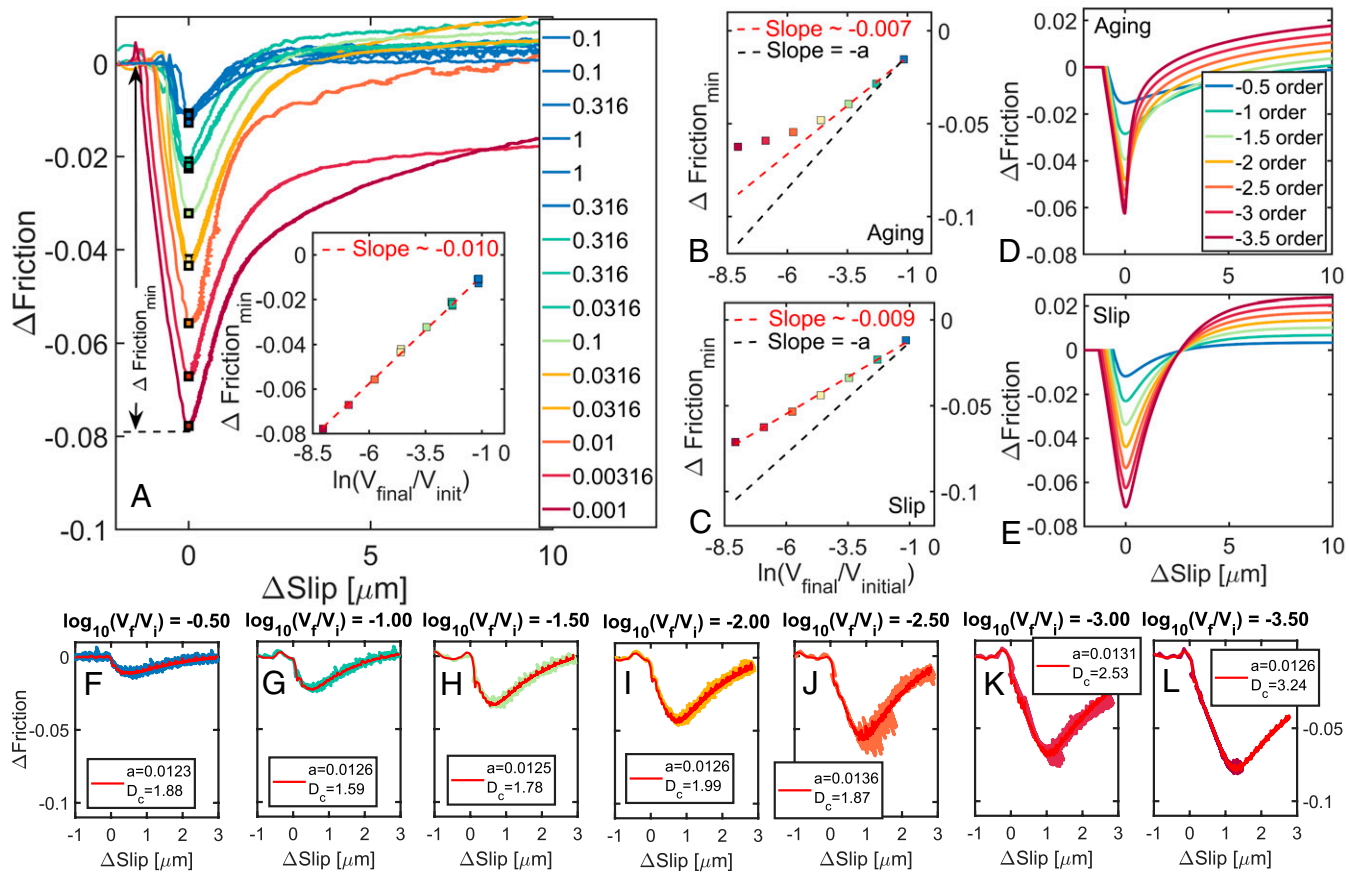


**Fig. 2.** (A) Same set of velocity-step decreases as in Fig. 1 color-coded identically according to  $\log_{10}(V_f/V_i)$ , but plotted as nonnormalized friction versus slip. The numbers in the legend show  $V_f$  in  $\mu\text{m} \cdot \text{s}^{-1}$ . Slip is set to zero at minimum stress, and shear stress is set to zero at the prestep level. The data are smoothed as in Fig. 1A. Inset shows the evolution of the stress minimum ( $\Delta \text{Friction}_{\min}$ ) with log step size. (B) Colored squares show stress minima following velocity-step decreases as a function of log step size, from the (smoothed) finite stiffness simulations in Fig. 1B for the Aging formulation (parameters from the red fits in *SI Appendix*, Fig. S8). The black dashed line has a slope of  $-a = -0.014$  (Table 1), which would be appropriate if there were no evolution of state prior to the stress minimum. The red dashed line is a fit to the three smallest simulated velocity steps. (C) Same as B, but for the Slip formulation (parameters from the fits in *SI Appendix*, Fig. S7); here,  $-a = -0.013$  (Table 1), and the red dashed line is a fit to all the velocity steps. Note that the Slip formulation predicts linear evolution of the stress minima with log step size, consistent with the laboratory data (red dashed line in A, Inset), albeit with a  $\sim 10\%$  shallower slope, while the Aging formulation predicts that the stress minima deviate to significantly shallower values from the initial linear trend as step size increases, due to increased state evolution. D and E show the evolution of friction for the Aging and Slip simulations of Fig. 1B and C, respectively, but referenced to the prestep steady value, as in A. F–L show Slip-formulation fits to one step of each size. Unlike the modeled friction minima in C, the fits in F–L are allowed to use different  $a$  and  $D_c$  ( $a - b$  for each is fixed at  $-0.003$ ) and are a subset of the fits to all the step decreases in *SI Appendix*, Fig. S9. Note the similarity in inferred  $a$  and  $D_c$  values across the steps and the excellent fit to the data.

of less than a factor of 2, to fit the whole suite of velocity-step decreases equally well. To the extent that the larger values of  $D_c$  for the two largest velocity steps might be statistically meaningful, note that this would imply an even slower rate of fault strengthening with slip for the largest velocity reductions, whereas time-dependent strengthening requires the opposite. However, the 95% CIs shown in *SI Appendix*, Fig. S11 seem to allow the possibility that any trends in  $D_c$  with step size are not significant.

While we have thus far focused on state evolution in response to velocity-step decreases, for completeness, we point out that the velocity-step increases in Fig. 1A also show systematic support for the Slip formulation. The data exhibit a quasi-characteristic length scale for stress evolution following the friction peak, independent of the sign as well as the size of the velocity step—a feature consistent with the Slip formulation (Fig. 1C) (28, 32–34). The Aging formulation, in contrast, predicts linear slip weakening postpeak for velocity-step increases that push the sliding surface far above steady state ( $V\theta/D_c \gg 1$ ) (28, 35) (Fig. 1B). Further, since the amplitude of the friction peak increases with step size, a constant rate of weakening implies that steady-state friction is attained over slip distances that also increase with step size—opposite to the trend predicted for step decreases. It is well established that such

asymmetry in the frictional response between large velocity-step increases and decreases is not supported by experiments (20, 22, 25, 28, 32, 36), and neither is it seen in our data.

Before concluding this section, we point out that most of our velocity-step increases and decreases show a long-term evolution in stress over slip distances much larger than the  $D_c$  derived by fitting the first few micrometers of slip following the step. Neither the Aging nor the Slip formulation can capture this feature with a single state variable (20, 25). This is the main reason we avoid fitting more than the first 3  $\mu\text{m}$  of slip following the step with our one-state variable models (*Materials and Methods*). Note that in obtaining the value  $a - b = -0.003$  (*SI Appendix*, Fig. S6), we use the steady-state values at more than 50  $\mu\text{m}$  of slip following our velocity steps. This value of  $a - b$  probably corresponds better to a two-state variable picture (25). But, on the other hand, the joint fit to the velocity steps in *SI Appendix*, Fig. S7, using the Slip formulation with a single state variable, requires  $a - b = -0.003$  without any a priori constraints. Given this, and for its analytical simplicity, we have restricted ourselves to the one-state-variable picture.

In summary, the fact that the data from far below steady state—both the preminimum stress decrease and the postminimum

increase—are so consistent with the Slip formulation over the first few micrometers of slip, where (for all but the largest step) most of the postminimum stress increase occurs, indicates that slip-dependent strengthening is responsible for most of the state evolution observed in these data. And, even when the data deviate from single-state-variable Slip-formulation predictions, as do the two largest step decreases, they do so by strengthening less rapidly with slip than predicted (see also *SI Appendix*, Fig. S7). This is still inconsistent with time-dependent strengthening, which predicts more rapid strengthening with slip in response to larger step decreases (*SI Appendix*).

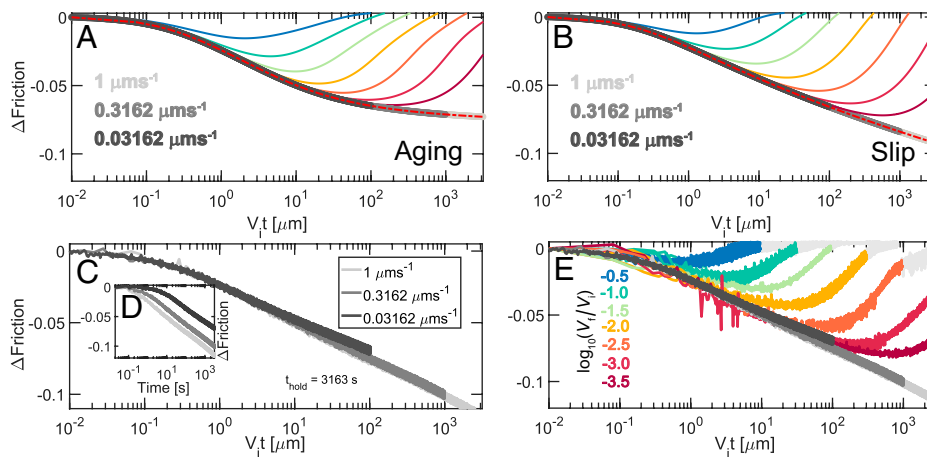
**Comparing Holds to the Large Velocity-Step Decreases.** Our study stands apart from previous work in that it analyzes velocity-step decreases and holds within a unified framework. For this reason, it is useful to examine the extent to which our largest velocity-step decreases and holds access similar sliding conditions. In Fig. 3, we compare the stress evolution in laboratory and simulated velocity-step decreases (solid colored lines) to that in holds (gray lines). Fig. 3 A and B show numerical simulations comparing the shear-stress relaxation during  $\sim 3,000$ -s holds from the different laboratory prehold driving rates we used ( $V_i = 1, 0.3$ , and  $0.03 \mu\text{m} \cdot \text{s}^{-1}$ ), to the shear-stress evolution following the different laboratory velocity-step sizes. In Fig. 3 C–E, we show corresponding laboratory hold and velocity-step data with Fig. 3 E being the analog of Fig. 3 A and B.

The simulations show that most of the stress decrease between the onset of the velocity steps and the subsequent friction minimum follow the stress-relaxation trajectory of the different load-point holds, when the data are plotted against rescaled time  $V_i t$ . This scaling removes any dependence of friction evolution on  $V_i$ , within the traditional RSF framework (i.e., constant  $a$ ,  $b$ , and  $D_c$  with no intrinsic velocity scale; *Materials and Methods*) (37, 38). Fig. 3C applies the same scaling to data from three  $\sim 3,000$ -s holds initiated at different  $V_i$  (Fig. 3D), and Fig. 3E adds to this all the velocity steps from Fig. 1A. Note that the measured stress relaxations across the entire suite of holds (gray curves) also collapse to a single trajectory in Fig. 3 C and D. This is a significant result, as it provides no evidence for the hypothesis that the RSF parameter values change substantially at sliding velocities

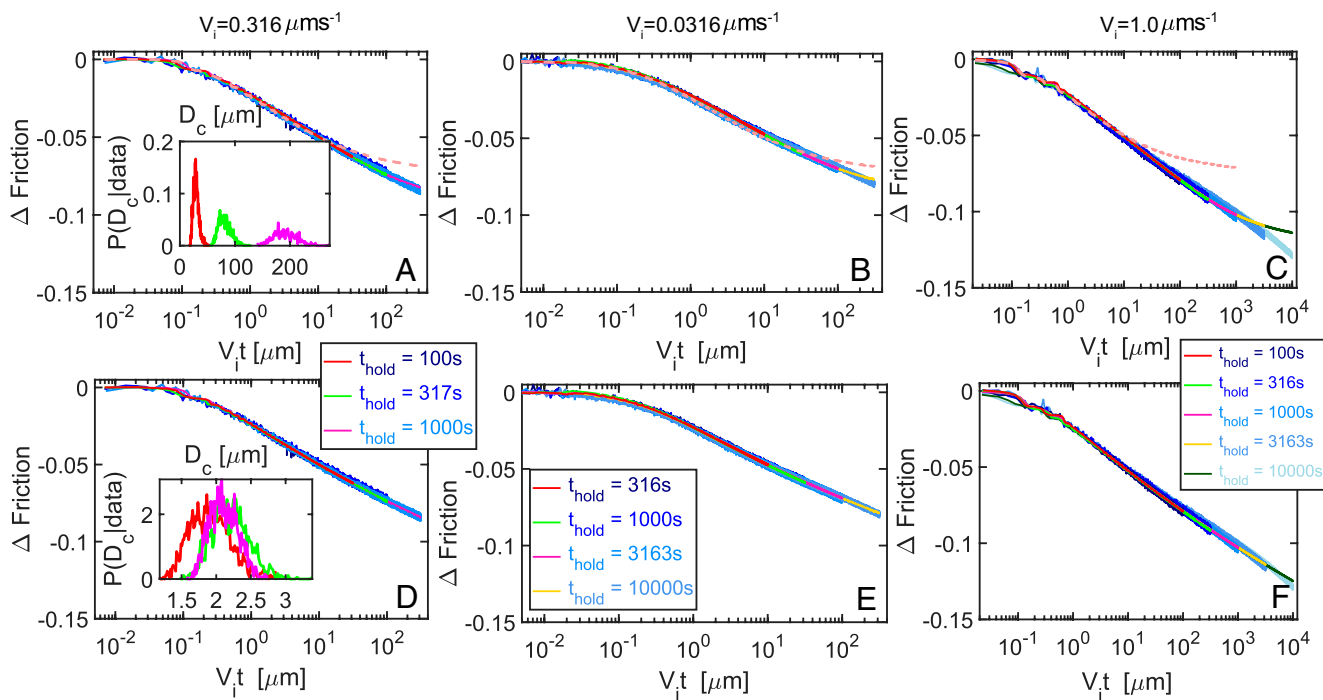
intermediate between  $V_i$  and the velocities reached by the ends of the holds (*Materials and Methods*).

Fig. 3 B and E show that the velocity steps and holds share friction phenomenology down to slip rates as low as those accessed by the largest velocity-step decreases ( $\sim 10^{-3} \mu\text{m} \cdot \text{s}^{-1}$ ). The longest holds then extend the slip rates accessed to values below  $10^{-5} \mu\text{m} \cdot \text{s}^{-1}$ . We show in the following section that these holds are fit well by the Slip formulation, using parameters very similar to those inferred from the velocity steps. *SI Appendix*, Fig. S15A shows that, for the Slip formulation, the largest velocity steps in our experiments access the same slip rates as holds of a few hundred seconds in duration, irrespective of their prehold sliding rates. This shows the utility of the large velocity-step decreases in our experiments—they clearly exhibit slip-dependent healing at the same sliding velocities achieved in holds long enough to clearly show logarithmic-in-time growth of both peak friction (4, 5) and contact area (10, 11).

**Slide-Hold Experiments.** Fits to our hold data (shown in Fig. 4) are all constrained with  $a - b = -0.003$ , as determined from the steady-state friction value as a function of sliding speed (*SI Appendix*, Fig. S6). Holds of all durations from a particular  $V_i$  were fit jointly. The only exceptions are those with  $V_i = 1 \mu\text{m} \cdot \text{s}^{-1}$  (Fig. 4 C and F), where we do not fit the two longest holds. For unknown reasons, and unlike the holds with  $V_i \sim 0.3$  and  $0.03 \mu\text{m} \cdot \text{s}^{-1}$  in the other panels, the longer holds with  $V_i = 1 \mu\text{m} \cdot \text{s}^{-1}$  do not track the trajectories of the nominally identical shorter holds over their shared duration. Fig. 4 A–C show fits using the Aging formulation. Although the fits up to modest values of  $V_i t$  ( $\lesssim 10^2 \mu\text{m}$ ) appear not too bad, they require values of  $D_c$  orders of magnitude larger than those inferred from the velocity steps (Table 1). To rationalize this feature of the fits, we note that under an Aging formulation with  $a < b$ , the rate of shear-stress relaxation in response to a load-point hold,  $d\tau/d\log(t)$ , decreases with time, ultimately vanishing in the limit  $V_i t \gg D_c$  (23). This is a direct implication of time-dependent strengthening ( $\dot{\theta} \sim 1$  far below steady state) and can be viewed as the “infinitely large step” limit of the pronounced shallowing of the friction minima, with increasing step size already seen in Fig. 2B. For  $a - b = -0.003$ , the Aging formulation



**Fig. 3.** Changes in friction, referenced to the prior steady-state value at slip speed  $V_i$ , for velocity-step decreases (solid colored lines) and holds (gray lines and dashed red line). The solid colored lines in A show the same finite stiffness simulations for the Aging formulation as in Fig. 1B, now plotted versus the logarithm of scaled time  $V_i t$ . The dashed red curve shows the stress-relaxation trajectories of a 3,000-s hold with  $V_i = 3 \mu\text{m} \cdot \text{s}^{-1}$  and the same  $a$ ,  $b$ , and  $D_c$  as the velocity steps. The gray curves are for the same parameters as the red dashed curve, except for the different indicated  $V_i$ . B is the same as A, but for the Slip formulation with its corresponding velocity-step-derived RSF parameters. C shows that the friction evolution during laboratory holds of 3,163 s at three different initial slip speeds from 0.03 to  $1 \mu\text{m}/\text{s}$  collapse onto nearly the same trajectory when plotted versus log-scaled time  $V_i t$ . D shows the same data when plotted as a function of time. E shows the same hold data and all the velocity-step-decrease data of Figs. 1 and 2, using the same scaling of time and color scheme as A and B. Initially, a sufficiently large load-point velocity reduction appears indistinguishable from a hold, and for both the models (A and B) and the data (E), the stress-decay trajectories for the holds and velocity steps closely track one another for as long as the sliding velocity  $V \gg V_f$ .



**Fig. 4.** Fits to the hold portions of the slide–hold–slide tests carried out during the same experimental run as the velocity steps in Fig. 1. The data are represented in various shades of blue, with lighter colors representing longer holds. The joint fits to all holds in each sequence are shown in the respective panels in colors other than blue. The friction change from the prior steady state is plotted as a function of scaled time  $V_i t$  as in Fig. 3. (A–C) Fits using the Aging formulation; note that these require unreasonably large values of  $D_c$  (Table 1). The dashed orange lines are predictions for the longest hold in the panel that was fit, using Aging parameters inferred from the velocity steps (Table 1). (D–F) Fits to the same holds, but now using the Slip formulation. The values of  $a$  and  $D_c$  required by the fits in D and E are nearly identical to those required to fit the velocity steps (Table 1 and *SI Appendix*, Fig. S7). The fit in F requires a  $D_c$  65% larger than that required to fit the velocity steps. *Insets* in A and D show the posterior distributions of  $D_c$  inferred from Monte Carlo inversions that fit the holds of different durations separately. Note that the Aging formulation requires progressively larger values of  $D_c$  for longer holds, while  $D_c$  inferred for the Slip formulation is statistically invariant across the range of hold durations. In C and F ( $V_i = 1.0 \mu\text{m} \cdot \text{s}^{-1}$ ), we did not fit the two longest holds because they showed very atypical behavior—concave-down friction versus log-time curves at long hold times and static friction peaks that decrease for hold durations longer than  $10^3$  s (F and *SI Appendix*, Fig. S16).

predicts that the shear-stress decay during holds begins to become significantly shallower than linear for  $V_i t / D_c \gtrsim 2$ , or  $V_i t \gtrsim 20$  for  $D_c \sim 10 \mu\text{m}$  (Fig. 3A). The hold data, however, show nearly log-linear stress relaxation for hold durations orders of magnitude larger than this. Therefore, an Aging formulation with  $a < b$  can produce good fits to these hold sequences only by requiring that  $D_c$  be not much smaller than the values of  $V_i t$  accessed during these holds.

Fig. 4A, *Inset* shows the distribution of  $D_c$  values estimated by using a Monte Carlo inversion method (*Materials and Methods*), obtained by fitting each of the three holds in the sequence individually. The inferred values of  $D_c$  increased with hold duration  $t_{\text{hold}}$ , as expected to satisfy the requirement that  $V_i t_{\text{hold}}$  not be much larger than  $D_c$ . For the same reason, the inferred values of  $D_c$  increased with  $V_i$  when fitting holds of the same duration in Fig. 4A–C (Table 1; the only exception to the latter statement is a second set of holds with  $V_i = 0.316 \mu\text{m} \cdot \text{s}^{-1}$  shown in *SI Appendix*, Fig. S16B).

To further evaluate the suitability of the Aging formulation to model these data, we utilize the velocity-weakening fit to the velocity steps obtained from the Aging formulation to numerically predict the stress relaxation during the longest hold in each panel (dashed orange lines in Fig. 4A–C). These numerical predictions significantly underestimated the shear-stress decrease observed during the longer holds. This is expected, given that the velocity steps are equivalent to hold durations much shorter than the longest holds at each  $V_i$  (for relevant Aging-equation predictions, see *SI Appendix*, Fig. S14A).

In contrast to the Aging formulation, the Slip formulation fits these holds very well (Fig. 4D–F), with parameters nearly

identical to those inferred from the velocity steps (Table 1). For the sets of holds in Fig. 4D and E, these Slip-equation fits capture the observed stress relaxation across the whole range of hold durations equally well with the same set of parameters. This is formally shown in Fig. 4D, *Inset*, where it can be seen that, in contrast to the Aging formulation, the distribution of acceptable values of  $D_c$  inferred by fitting each of the three holds in the sequence individually are statistically equivalent. For the set of holds in Fig. 4F, as noted previously, only the three shortest holds were fit. The  $D_c$  inferred from this set of holds is about twice as large as those in Fig. 4D and E, within the range of variation in  $D_c$  inferred when all the velocity steps are fit independently (*SI Appendix*, Fig. S11).

So, overall, and consistent with the findings of ref. 23, the Slip-equation fits to the internally consistent holds in Fig. 4D and E capture the stress relaxation at the longest hold times better than the corresponding Aging-equation fits. The good Slip-equation fit to the shear-stress data at such low slip rates (as low as  $0.02 \text{ nm} \cdot \text{s}^{-1}$ ; *SI Appendix*, Fig. S5) implies, remarkably, that state evolution in these experiments is controlled by slip, rather than elapsed time, even at rates more than an order of magnitude below plate tectonic rates.

Before finishing this discussion, we point out that, unlike the holds, the corresponding reslides are not well modeled by either the Slip or the Aging formulation (*SI Appendix*, Figs. S17–S19). For example, the Slip-equation fits to the holds in Fig. 4D–F fail to match most of the static friction peaks upon resliding, reach those peaks after less slip than the laboratory data (*SI Appendix*, Fig. S17), and, following the peak, approach steady-state friction much more quickly than the data [*SI Appendix*,

Fig. S18 (39)]. Therefore, although the Slip version appears to do a much better job, neither of these widely used empirical formulations fit the entire range of laboratory data.

## Discussion

Traditionally, the hold portions of slide–hold–reslide experiments have been interpreted as loosely analogous to the interseismic period between earthquakes, with the reslide portion being more appropriate to the rapid acceleration prior to dynamic slip. In numerical simulations, the response of the adopted state-evolution equation to reslides controls the length scale and style of earthquake nucleation, as it controls the transition from “static” to “dynamic” friction and the fracture energy of the nucleation zone (34). The stress decay during load-point holds is potentially relevant to the magnitude and time history of postseismic slip, which can be monitored geodetically. However, the many differences between natural faults and laboratory experiments complicate such analogies, including reactive pore fluid flow (40) and the fact that laboratory holds start from friction levels appropriate for steady sliding at low speeds, whereas the interseismic period on natural faults might start with very low friction values associated with thermal weakening during the prior earthquake (41). For such reasons, directly translating the results of laboratory rock-friction experiments to natural faults is a fraught endeavor. Our more limited goal here has been to better understand those laboratory experiments that underlie essentially all modern simulations of fault slip at less than dynamic speeds.

More specifically, our goal has been to determine whether the frictional strengthening of surfaces sliding at conditions far below steady state is dominantly slip-dependent or time-dependent. For both velocity-step decreases and slide–hold laboratory protocols, we have established that the surface strengthens (that is, state increases) primarily with slip. In doing so, we have also demonstrated that the conventional (but self-contradictory) wisdom that state evolution in response to velocity-step decreases is slip-dependent, while that in response to load-point holds is time-dependent, is incorrect. Instead, by treating holds as the limit of increasingly large velocity-step decreases, we have shown that the phenomenology of frictional healing is not only slip-dependent, but is well explained by the standard Slip formulation to within a few tens of percent of variation in the RSF parameters. This consistency is observed across more than 5 orders of magnitude variation in slip rate from  $3 \mu\text{m} \cdot \text{s}^{-1}$  to  $< 10^{-5} \mu\text{m} \cdot \text{s}^{-1}$ .

In contrast, we have shown that any formulation in which the state contribution to friction increases as log time, analogously to the log-time contact-area growth observed at low slip rates, makes the interface too strong to match the stress relaxation observed during both load-point holds and, prior to their stress minima, step-velocity decreases. The Aging equation is a particular example of such a formulation.

In this context, it is worth remembering that log-time growth of contact area is not only well established in observations in transparent materials (10, 11), but it also has a well-accepted theoretical basis (42). In rock, the same log-time growth of contact area has been inferred from proxy measurements of fault-normal displacement and acoustic transmissivity during load-point holds (31, 43) or from log-time compaction of granular wear material accumulated on initially bare rock interfaces (44). Therefore, it is quite remarkable how poorly the Aging formulation performs in reproducing friction evolution during holds, even though it mimics very well the observed phenomenology of contact-area growth under similar conditions. Our results, thus, add to a

growing body of evidence that the evolution of state embodies more than just changes in contact area (45–47).\*

The bigger surprise is the extreme slip-sensitivity of friction at even subnanometric slip rates. Several underlying mechanisms could give rise to slip-dependent state evolution. Asperities might retain a memory of the velocity(ies) at which they formed, in which case reaching a new steady state might require swapping out the old contacts for the new, regardless of how long that takes (48). Additionally, contact area might grow during holds or normal stress increases, but that new contact area might have to undergo some strain-hardening (via slip) before reaching its steady-state strength (47). Although these ideas have been explored numerically (48, 49), no formulation developed thus far does better than the Slip formulation in describing laboratory friction data.

However, recent Discrete Element Method (DEM) simulations of a granular gouge layer sheared between two parallel plates, as a model for fault friction, behaved very similar to the Slip formulation, with nearly constant RSF parameters during velocity-step and slide–hold protocols, consistent with laboratory experiments (50). The model gouge also underwent log-time compaction during the holds, meaning that the DEM simulations share with laboratory experiments the property that, although the interface normal displacements are seemingly consistent with the conventional understanding of the Aging formulation, the simulated shear-stress decay follows the Slip formulation. Although these simulation results appear quite promising, the microscopic mechanisms giving rise to the macroscopically laboratory-like behavior remain unknown. However, granular systems are known to exhibit the same slow dynamics of other disordered systems near the “glass-transition temperature,” behavior that has previously been invoked to explain nonmonotonic contact-area changes in poly (methyl methacrylate) (PMMA) at times of constant normal load (51).

It is possible, even likely, that at slip rates even lower than those accessed in our experiments, some additional process that involves time-dependent healing also contributes to frictional strengthening. For example, it is known that interfaces continue to strengthen, even when held truly stationary by unloading to zero shear stress (3, 6, 21, 52). One proposed state-evolution equation (24), originally intended to reconcile the apparent slip-versus-time discrepancy between velocity step and slide–hold–reslide experiments, posits a transition from slip-dependent to time-dependent strengthening as the slip speed drops below some critical value. Our data show that this critical velocity, if it exists, must lie below the range of slip speeds accessed by our slide–hold–reslide experiments [if it did not, kinks would be produced in the curves of stress decay and peak stress as a function of log-hold time, kinks that are absent from laboratory data (23)]. And, as we noted previously, our slide–hold–reslide experiments access sliding velocities well below plate tectonic rates.

It is also important to note that while the Slip formulation fits our velocity steps and holds with nearly identical parameters, it fails to fit the stress history following the initiation of the reslide. In all cases, detectable slip begins to accumulate at lower stress levels than predicted (SI Appendix, Fig. S17 A–C), as if the laboratory sample undergoes unmodeled weakening early on during the reslides. Despite this, the peak friction achieved in the laboratory sample in most cases exceeds the predicted value, by up to a few tens of percent (SI Appendix, Fig. S17 D–F), as if unmodeled strengthening later during the reslide overcomes

\*T. E. Tullis, P. Bhattacharya, A. Rubin, N. Badt, N. Beeler, “Analysis of normal stress stepping experiments indicates that friction evolution depends on contact area quality rather than quantity” in American Geophysical Union, Fall Meeting 2019 (2020).

this initial weakening. These observations may indicate that the interface undergoes structural changes during the rapid stress increase of the reslide, changes that are not captured by any existing state-evolution formulation. Insight into these changes might come from granular flow simulations, which have successfully reproduced several aspects of laboratory rock and gouge friction experiments (50, 53), and examination of the time-dependent normal displacement across the sliding surface. Nonetheless, the Slip formulation appears to do a better job of matching the peak friction during the reslides than the Aging formulation, which predicts that  $\Delta\mu_{peak}$ , when plotted versus  $\ln(t_{hold})$ , has a slope of  $b$ , which is well constrained by our velocity steps. The observed slope is smaller by about a factor of 3 (SI Appendix, Fig. S17 D and E), a discrepancy that has been seen previously (54).

What also remains to be examined is the extent to which this phenomenology of rock friction extends to other materials. The clearest evidence for log-time contact-area growth comes from transparent acrylic (PMMA), but PMMA samples have yet to be subjected to as exhaustive of a set of sliding conditions as reported in this manuscript. This wide range of conditions has proven to be necessary to distinguish between time-dependent and slip-dependent strengthening for surfaces far below steady state. Experiments that leverage simultaneous measurements of contact area and stresses under extreme deviations from steady state could provide unprecedented details about the association of contact area and strength. A comprehensive study of the universality of friction phenomenology, among other important natural and industrial materials, is necessary, particularly given the diversity of materials and purposes across which RSF is used—elastomers to plastics/acrylics to metals to soft materials and micromachines (6, 15, 16, 55, 56).

Given that state must, in general, depend upon both contact area and the quality of chemical bonding across those contacts (45, 46, 57, 58), it would be surprising if friction could be accurately described by a single state variable. It is, thus, remarkable that the empirical Slip formulation for state evolution does as well as it does, fitting velocity steps of both signs and load-point holds with near-identical parameters. This suggests that it is a good starting point for developing a state-evolution formulation to better fit the reslides after holds. This is in contrast to earlier attempts at revising state-evolution equations that considered time-dependent strengthening, as embodied by the Aging formulation, to be a desirable property of state evolution at low slip rates (24, 31). Our results, instead, show that this is the portion of the parameter space where time-dependent strengthening descriptions, such as the Aging formulation, are least compatible with laboratory friction data.

## Materials and Methods

**Estimating Stiffness and  $a - b$  from Independent Constraints.** Our experiments were carried out on the Tullis rotary shear apparatus at Brown University, which was artificially stiffened by using servo feedback from a near-fault transducer. To obtain an estimate of this higher stiffness, we used the initial loading curve of the reslides, following a sequence of long holds carried out during the same experimental run. At the end of long holds, the block was sliding at rates orders-of-magnitude smaller than the prehold steady sliding rate  $V_i$ . Therefore, following the reslide, also at the rate  $V_i$ , there is an initial time window over which the slip rate of the block continues to satisfy  $V \ll V_i$ . During this initial portion of the reload, assuming quasi-static force balance between the driving shear stress and friction, we have

$$\Delta\mu = k(\delta_{lp} - \delta) = k\delta_{lp} \left(1 - \frac{\delta}{\delta_{lp}}\right) \approx k\delta_{lp}, \quad [5]$$

where  $\delta$  and  $\delta_{lp}$  are surface and load-point displacements since the reslide, respectively, and initially  $\delta/\delta_{lp} \ll 1$  for reslides following long holds. Note that  $k$  is the stiffness normalized by normal stress, and  $\Delta\mu$  is the change in friction. A linear fit to the  $\Delta\mu$  versus  $\delta_{lp}$  plot over this initial portion following the reslide gives  $k$  as the slope (SI Appendix, Fig. S4). We use the reslides following a sequence of 3,000-s and 10,000-s holds carried out at three different values of  $V_i$ , spanning more than an order of magnitude—1, 0.3162, and 0.03162  $\mu\text{m} \cdot \text{s}^{-1}$ . For the linear fit, we chose one-seventh of the total number of points between the onset of the reslide and eventual peak strength to evaluate  $k$ . This fraction was chosen based on trial-and-error, such that the spread in the estimated value of  $k$  was the least between our six chosen reslides. We found  $k \sim 0.065 \mu\text{m}^{-1}$  to be the mean stiffness from our fits.

For constant RSF parameters, the slope of the curve of steady-state friction versus  $\ln(V)$  is equal to  $(a - b)$ . In SI Appendix, Fig. S6, we show the estimation of  $a - b$  from all the 0.5- to 2.0-order velocity steps in Fig. 1A. The poststep steady state is chosen for all steps at 45  $\mu\text{m}$  of postminimum slip (brown stars in each panel). We did not use larger steps for  $a - b$  estimation because of the prominent postminimum transients present at 45- $\mu\text{m}$  slip distance for these steps. We find that  $a - b \sim -0.003$  explains the data well from the 3  $\mu\text{m} \cdot \text{s}^{-1}$  to 0.03  $\mu\text{m} \cdot \text{s}^{-1}$  slip rates covered between these steps.

**Estimating  $a$  and  $D_c$  by Fitting the Velocity-Step Decreases.** To constrain  $a$  and  $D_c$ , we fit either a representative size range of the velocity-step decreases (3.5 to 1 orders of magnitude) or all of the velocity steps in Fig. 1A with the Slip equation. The forward model was simulated by equating the time derivative of  $\Delta\mu$  in Eq. 5 (using the load-point displacement history recorded during the experiment and  $k = 0.065 \mu\text{m}^{-1}$ ) with that in the friction law (Eq. 1), with the Slip equation being used for state evolution (Eq. 2b). All data were sampled uniformly at 50 Hz in these experiments. We fit the velocity-step decreases in two ways—1) parameters  $a$ ,  $b$ , and  $D_c$  were simultaneously and jointly inferred from all the velocity-step decreases shown in SI Appendix, Fig. S7 A-E; and 2) parameters  $a$  and  $D_c$  were inferred independently by fitting all the velocity steps individually with the constraint that  $a - b = -0.003$  (SI Appendix, Fig. S9 A-O). For the fits of type 1, we weighted the misfit for each velocity step by the inverse of the total number of data samples in the fitting window to ensure that the data from all the velocity steps contributed equally to the aggregate misfit. For the inversion, we used an adaptive-proposal, small-world, Markov chain Monte Carlo code. The algorithm and the general inversion procedure are described in the supplementary materials accompanying ref. 22. We minimized the weighted square-root misfit between the modeled time series and the data at every time sample in the data. We modeled the evolution of friction only over the first 3  $\mu\text{m}$  of slip after the onset of the velocity step. This avoids fitting secondary long-term transients in the evolution of friction present in the data. For completeness, we carried out a set of Aging-equation fits for all the velocity steps in Fig. 1 jointly with the same  $a$  and  $D_c$  (see SI Appendix, Fig. S8 for details). The inferred  $a$  and  $D_c$  values are reported in Table 1.

**Scaling of Friction Response of Holds and Steps from Different Initial Velocities under Single-State-Variable RSF.** RSF with constant parameter values and no intrinsic velocity scale predicts that friction evolution is independent of the prestep or prehold sliding rate  $V_i$ , when time is rescaled as  $V_i t$ . To show this, we begin by generalizing Eq. 1 to two-state variables and use  $V_i$  for the arbitrary reference velocity  $V_*$ :

$$\mu = \frac{\tau_f}{\sigma} = \mu_* + a \ln \left( \frac{V}{V_i} \right) + b_1 \ln \left( \frac{V_i \theta_1}{D_1} \right) + b_2 \ln \left( \frac{V_i \theta_2}{D_2} \right), \quad [6]$$

(extension to additional state variables is straightforward). We assume, as in Eqs. 2, that the evolution equation for each  $\theta_n$  can be expressed as a function of the dimensionless parameter  $V\theta_n/D_n$ :

$$\frac{d\theta_1}{dt} = F \left( \frac{V\theta_1}{D_1} \right); \frac{d\theta_2}{dt} = F \left( \frac{V\theta_2}{D_2} \right). \quad [7]$$

To obtain an evolution equation for  $V$  following a velocity step or hold, dividing [3] by  $\sigma$ , equating this to the right-hand side of [6], and taking the time derivative yields

$$\frac{dV}{dt} = V \frac{b_1}{a} \left[ \frac{k}{b_1} (V_f - V) - \frac{\dot{\theta}_1}{\theta_1} - \frac{b_2}{b_1} \frac{\dot{\theta}_2}{\theta_2} \right], \quad [8]$$

where  $V_f$  is the poststep load-point velocity (zero for a hold). Next, we make [7] and [8] dimensionless by normalizing velocities by  $V_i$  and time (as well as  $\theta_1$  and  $\theta_2$ ) by  $D_1/V_i$ :

$$\frac{d\tilde{\theta}_1}{d\tilde{t}} = F(\tilde{V}\tilde{\theta}_1); \frac{d\tilde{\theta}_2}{d\tilde{t}} = F(\tilde{V}\tilde{\theta}_2, \frac{D_1}{D_2}); \quad [9]$$

$$\frac{d\tilde{V}}{d\tilde{t}} = \tilde{V} \frac{b_1}{a} \left[ \frac{kD_1}{b_1} \left( \frac{V_f}{V_i} - \tilde{V} \right) - \frac{d\tilde{\theta}_1/d\tilde{t}}{\tilde{\theta}_1} - \frac{b_2}{b_1} \frac{d\tilde{\theta}_2/d\tilde{t}}{\tilde{\theta}_2} \right]; \quad [10]$$

where tildes represent dimensionless variables. Assuming steady-state sliding before the step/hold, the initial conditions on  $\theta$  at the time of the step are

$$\tilde{\theta}_1 \Big|_{\tilde{t}=0} = 1; \tilde{\theta}_2 \Big|_{\tilde{t}=0} = \frac{D_2}{D_1}. \quad [11]$$

Eqs. 9–11 show that, provided the RSF parameters  $a, b_n$ , and  $D_n$  are independent of sliding speed,  $\tilde{V}(\tilde{t})$  and  $\tilde{\theta}_n(\tilde{t})$  depend upon  $V_f/V_i$  (term in parentheses in [10]), but do not depend on  $V_i$  independently. Furthermore, taking the time-derivative of Eq. 3 and equating  $\mu$  with  $\tau/\sigma$ ,

$$\frac{d\mu}{d(V_i t)} = k \left( \frac{V_f}{V_i} - \tilde{V} \right). \quad [12]$$

As both terms within the parentheses on the right side of [12] depend only upon  $V_f/V_i$ , again provided the RSF parameters are constant, plots of the friction change during holds should be independent of  $V_i$  when plotted versus scaled time  $V_i t$ . In addition, velocity-step decreases should be indistinguishable from holds as long as  $V \gg V_f$ . Thus, the generally clean overlap of the stress-relaxation

1. J. H. Dieterich, Time-dependent friction in rocks. *J. Geophys. Res.* **77**, 3690–3697 (1972).
2. J. H. Dieterich, Time-dependent friction and the mechanics of stick-slip. *Pure Appl. Geophys.* **116**, 790–806 (1978).
3. M. Nakatani, H. Mochizuki, Effects of shear stress applied to surfaces in stationary contact on rock friction. *Geophys. Res. Lett.* **23**, 869–872 (1996).
4. N. Beeler, T. E. Tullis, J. D. Weeks, The roles of time and displacement in the evolution effect in rock friction. *Geophys. Res. Lett.* **21**, 1987–1990 (1994).
5. C. Marone, Laboratory derived friction laws and their application to seismic faulting. *Annu. Rev. Earth Planet. Sci.* **26**, 643–696 (1998).
6. P. Berthoud, T. Baumberger, C. G'Sell, J. M. Hiver, Physical analysis of the state- and rate-dependent friction law: Static friction. *Phys. Rev. B Condens. Matter Mater. Phys.* **59**, 14313–14327 (1999).
7. S. L. Karner, C. Marone, Frictional restrengthening in simulated fault gouge: Effect of shear load perturbations. *J. Geophys. Res. Solid Earth* **106** (B9), 19319–19337 (2001).
8. T. Baumberger, C. Caroli, Solid friction from stick-slip down to pinning and aging. *Adv. Phys.* **55**, 279–348 (2006).
9. C. Marone, The effect of loading rate on static friction and the rate of fault healing during the earthquake cycle. *Nature* **391**, 69–72 (1998).
10. J. H. Dieterich, B. D. Kilgore, Direct observation of frictional contacts: New insights for state-dependent properties. *Pure Appl. Geophys.* **143**, 283–302 (1994).
11. O. Ben-David, S. M. Rubinstein, J. Fineberg, Slip-stick and the evolution of frictional strength. *Nature* **463**, 76–79 (2010).
12. F. P. Bowden, D. Tabor, *The Friction and Lubrication of Solids, Part 2* (Oxford University Press, New York, 1964).
13. Y. Brechet, Y. Estrin, The effect of strain rate sensitivity on dynamic friction of metals. *Scr. Metall. Mater.* **30**, 1449–1454 (1994).
14. J. H. Dieterich, Modeling of rock friction: 1. Experimental results and constitutive equations. *J. Geophys. Res.* **84**, 2161–2168 (1979).
15. V. Prakash, Frictional response of sliding interfaces subjected to time varying normal pressures. *J. Tribol.* **120**, 97–102 (1998).
16. O. Ronsin, K. L. Coeyrehourcq, State, rate and temperature-dependent sliding friction of elastomers. *Proc. Royal Soc. Ser. A: Math. Phys. Eng. Sci.* **457**, 1277–1294 (2001).
17. S. S. Shroff, N. Ansari, W. Robert Ashurst, M. P. de Boer, Rate-state friction in microelectromechanical systems interfaces: Experiment and theory. *J. Appl. Phys.* **116**, 244902 (2014).
18. F. Heslot, T. Baumberger, B. Perrin, B. Caroli, C. Caroli, Creep, stick-slip, and dry-friction dynamics: Experiments and a heuristic model. *Phys. Rev. E Stat. Phys. Plasmas Fluids Relat. Interdiscip. Topics* **49**, 4973–4988 (1994).
19. J. M. Carlson, A. A. Batista, Constitutive relation for the friction between lubricated surfaces. *Phys. Rev. E Stat. Phys. Plasmas Fluids Relat. Interdiscip. Topics* **53**, 4153–4165 (1996).
20. A. Ruina, Slip instability and state variable friction laws. *J. Geophys. Res.* **88**, 10359–10370 (1983).
21. L. Bureau, T. Baumberger, C. Caroli, Rheological aging and rejuvenation in solid friction contacts. *Eur. Phys. J. E Soft Matter* **8**, 331–337 (2002).
22. P. Bhattacharya, A. M. Rubin, E. Bayart, H. M. Savage, C. Marone, Critical evaluation of state evolution laws in rate and state friction: Fitting large velocity steps in simulated fault gouge with time-, slip-, and stress-dependent constitutive laws. *J. Geophys. Res.: Solid Earth* **120**, 6365–6385 (2015).
23. P. Bhattacharya, A. M. Rubin, N. M. Beeler, Does fault strengthening in laboratory rock friction experiments really depend primarily upon time and not slip? *J. Geophys. Res.: Solid Earth* **122**, 6389–6430 (2017).
24. N. Kato, T. E. Tullis, A composite rate- and state-dependent law for rock friction. *Geophys. Res. Lett.* **28**, 1103–1106 (2001).
25. T. E. Tullis, J. D. Weeks, Constitutive behavior and stability of frictional sliding of granite. *Pure Appl. Geophys.* **124**, 383–414 (1986).
26. M. L. Blanpied, C. J. Marone, D. A. Lockner, J. D. Byerlee, D. P. King, Quantitative measure of the variation in fault rheology due to fluid-rock interactions. *J. Geophys. Res.* **103** (B5), 9691–9712 (1998).
27. J. R. Rice, N. Lapusta, K. Ranjith, Rate and state dependent friction and the stability of sliding between elastically deformable solids. *J. Mech. Phys. Solids* **49**, 1865–1898.
28. M. Nakatani, Conceptual and physical clarification of rate and state friction: Frictional sliding as a thermally activated rheology. *J. Geophys. Res.* **106** (B7), 13347–13380 (2001).
29. N. M. Beeler, T. E. Tullis, M. L. Blanpied, J. D. Weeks, Frictional behavior of large displacement experimental faults. *J. Geophys. Res. Solid Earth* **101** (B4), 8697–8715 (1996).
30. T. E. Tullis, "Friction measurement apparatus" in *Instruments of Science: An Historical Encyclopedia*, R. F. Bud, D. J. Warner, Eds. (Garland, New York, 1997), pp. 249–251.
31. K. Nagata, M. Nakatani, S. Yoshida, A revised rate- and state-dependent friction law obtained by constraining constitutive and evolution laws separately with laboratory data. *J. Geophys. Res.* **117**, B02314 (2012).
32. M. F. Linker, J. H. Dieterich, Effects of variable normal stress on rock friction: Observations and constitutive equations. *J. Geophys. Res.* **97** (B4), 4923–4940 (1992).
33. J. R. Rice, Spatio-temporal complexity of slip on a fault. *J. Geophys. Res.* **98** (B6), 98859907 (1993).
34. J. P. Ampuero, A. M. Rubin, Earthquake nucleation on rate and state faults—aging and slip laws. *J. Geophys. Res.* **113**, B01302 (2008).
35. A. M. Rubin, J. P. Ampuero, Earthquake nucleation on (aging) rate and state faults. *J. Geophys. Res.* **110**, B11312 (2005).
36. A. Ruina, Ph.D. thesis (Division of Engineering, Brown University, Providence, RI) (1980).
37. K. Ranjith, J. Rice, Stability of quasi-static slip in a single degree of freedom elastic system with rate and state dependent friction. *J. Mech. Phys. Solids* **47**, 1207–1218 (1998).
38. J. C. Gu, J. R. Rice, A. L. Ruina, S. T. Tse, Slip motion and stability of a single degree of freedom elastic system with rate and state dependent friction. *J. Mech. Phys. Solids* **32**, 167–196 (1984).
39. N. M. Beeler, A. Rubin, P. Bhattacharya, K. Kilgore, T. Tullis, Apparent age dependence of the fault weakening distance in rock friction. *J. Geophys. Res. Solid Earth* **127**, e2021JB022772 (2022).
40. J. Chen, C. J. Spiers, Rate and state frictional and healing behavior of carbonate fault gouge explained using microphysical model. *J. Geophys. Res. Solid Earth* **121**, 8642–8665 (2016).
41. J. R. Rice, Heating and weakening of faults during earthquake slip. *J. Geophys. Res. Solid Earth* **111** (B5), (2006).
42. P. Berthoud, T. Baumberger, Shear stiffness of a solid-solid multicontact interface. *Proc. R. Soc. London A Math. Phys. Engineering Sci.* **454**, 1615–1634 (1998).
43. K. Nagata, B. D. Kilgore, N. Beeler, M. Nakatani, High-frequency imaging of elastic contrast and contact area with implications for naturally observed changes in fault properties. *J. Geophys. Res. Solid Earth* **119**, 5855–5875 (2014).
44. N. M. Beeler, T. E. Tullis, The roles of time and displacement in velocity-dependent volumetric strain of fault zones. *J. Geophys. Res. Solid Earth* **102** (B10), 22595–22609 (1997).
45. Q. Li, T. E. Tullis, D. Goldsby, R. W. Carpick, Frictional ageing from interfacial bonding and the origins of rate and state friction. *Nature* **480**, 233–236 (2011).
46. C. A. Thom, R. W. Carpick, D. L. Goldsby, Constraints on the physical mechanism of frictional aging from nanoindentation. *Geophys. Res. Lett.* **45**, 13306–13311 (2018).
47. B. D. Kilgore, J. Lozos, N. Beeler, D. Ogleby, Laboratory observations of fault strength in response to changes in normal stress. *J. Appl. Mech.* **79**, 31007 (2012).
48. T. Li, A. M. Rubin, A microscopic model of rate and state friction evolution. *J. Geophys. Res. Solid Earth* **122**, 6431–6453 (2017).
49. T. Li, An effort to reconcile time- and slip-dependent friction evolution. *J. Geophys. Res. Solid Earth* **124**, 1838–1851 (2019).
50. B. Ferdousi, A. M. Rubin, A granular physics-based view of fault friction experiments. *J. Geophys. Res. Solid Earth* **125**, e2019JB019016 (2020).

trajectories during the holds in Fig. 3C is consistent with the RSF parameters being nearly constant across the >5-orders-of-magnitude range of velocities accessed in these experiments.

**Data Availability.** Data from friction experiments have been deposited in Zenodo ([10.5281/zenodo.5596453](https://doi.org/10.5281/zenodo.5596453)) (59).

**ACKNOWLEDGMENTS.** Support for P.B. came from his start-up grant from the National Institute of Science Education and Research. Support for A.M.R. came from NSF Grant EAR1547286. Financial support from two sources kept the Brown University laboratory operational during the time these experiments were conducted. Support derived from NSF Grant EAR1359596 and Southern California Earthquake Center (SCEC) Grant 16026 (SCEC Contribution 9952) is acknowledged. SCEC is funded by NSF Cooperative Agreement EAR-1600087 and US Geological Survey Cooperative Agreement G17AC00047. Reviews from Nicholas van der Elst and Sam Dillavou prior to submission and three anonymous referees during the PNAS review process helped improve the paper to a considerable extent. Any use of trade, firm, or product names is for descriptive purposes only and does not imply endorsement by the US Government.

Author affiliations: <sup>a</sup>School of Earth and Planetary Sciences, National Institute of Science Education and Research (NISER), Bhubaneswar, 752050, India; <sup>b</sup>Department of Geosciences, Princeton University, Princeton, NJ 08544; <sup>c</sup>Department of Earth, Environmental, and Planetary Sciences, Brown University, Providence, RI 02912; <sup>d</sup>Cascades Observatory, US Geological Survey, Vancouver, WA 98683; <sup>e</sup>Kochi Institute for Core Sample Research, Japan Agency for Marine-Earth Science and Technology (X-star), JAMSTEC, Kochi 739-8502, Japan; and <sup>f</sup>Earth and Planetary Systems Science Program, Graduate School of Advanced Science and Engineering, Hiroshima University, Hiroshima 739-8526, Japan

51. S. Dillavou, S. M. Rubinstein, Nonmonotonic aging and memory in a frictional interface. *Phys. Rev. Lett.* **120**, 224101 (2018).
52. S. L. Karner, C. Marone, The effect of shear load on frictional healing in simulated fault gouge. *Geophys. Res. Lett.* **25**, 4561–4564 (1998).
53. B. Ferdowsi, A. M. Rubin, Slide-hold-slide protocols and frictional healing in discrete element method (DEM) simulations of granular fault gouge. *J. Geophys. Res. Solid Earth* **126**, e2021JB022125 (2021).
54. M. J. Ikari, B. M. Carpenter, C. Marone, A microphysical interpretation of rate- and state-dependent friction for fault gouge. *Geochem. Geophys. Geosyst.* **17**, 1660–1677 (2016).
55. S. S. Shroff, M. P. de Boer, Full assessment of micromachine friction within the rate-state framework: Theory and validation. *Tribol. Lett.* **63**, 39 (2016).
56. R. Sahli et al., Evolution of real contact area under shear and the value of static friction of soft materials. *Proc. Natl. Acad. Sci. U.S.A.* **115**, 471–476 (2018).
57. B. Weber, T. Suhina, A. M. Brouwer, D. Bonn, Frictional weakening of slip interfaces. *Sci. Adv.* **5**, eaav7603 (2019).
58. K. Tian, D. L. Goldsby, R. W. Carpick, Rate and state friction relation for nanoscale contacts: Thermally activated Prandtl-Tomlinson model with chemical aging. *Phys. Rev. Lett.* **120**, 186101 (2018).
59. P. Bhattacharya, A. M. Rubin, T. E. Tullis, N. B. Beeler, K. Okazaki, Data from "The evolution of rock friction is more sensitive to slip than elapsed time, even at near-zero slip rates." Zenodo. <https://zenodo.org/record/5596453#.YtFxgHbMLcs>. Deposited 25 October 2021.